RMIB GERB Processing: Angular Dependency Models

Nicolas Clerbaux, Steven Dewitte, Cedric Bertrand

13th February 2006

MSG-RMIB-GE-TN-0008, Version 2.0

Abstract

This technical note describes the radiance–to–flux conversions implemented in the RMIB GERB Processing (RGP). It consists in 2 different parts: (i) the thermal conversion based on theoretical model developped at RMIB and (ii) the solar conversion based on the RGP scene identification and the CERES-TRMM ADM's.

Contents

CHANGE RECORD

Issue	Date	Approved by	Reason for change
Version 1	08/07/1999		new document
Version 1.1	29/09/1999		CDR review
Version 2.0	07/02/2006		Update for data release

1 Introduction - Purpose of this document

The purpose of this document is to give a detailed overview of the methods and algorithms used to convert the Geostationary Earth Radiation Budget (GERB, Harries and GIST, 2005) unfiltered radiances -the measurement in the direction of the satellite- into the corresponding fluxes -the upper-hemisphere integration.

The document contains 2 well-separated parts: §3 and §4 present the angular dependency models for the thermally emitted and solar reflected radiation, respectively.

2 Acronyms, abbreviations and definitions

2.1 Acronyms and abbreviations

Not all these acronyms may appear in this document.

AD	Applicable Document
ADM	Angular Dependency Model
ASI	Agency Spatiale Italiano
BATS	Belgian Advanced Technology Systems
BB	Broad Band
BDRF	Bidirectional Reflection Function
CERES	Clouds and the Earth's Radiant Energy System
CNRS	Centre Nationale de la Recherche Scientifique
DCT	Discrete Cosine Transform
ERB	Earth Radiation Budget
ERBE	Earth Radiation Budget Experiment
EUMETSAT	EUropean organsiation for the exploitation of METeorological SATellites
FTP	File Transfer Protocol
Gb	Gigabit
GB	GigaByte
GERB	Geostationary Earth Radiation Budget
GGSPS	GERB Ground Segment Processing System
GIST	GERB International Science Team
GKSS	GKSS research centre
HD	High Density
HDF	Hierarchical Data Format
HRIT	High Rate Information Transmission
ICD	Interface Control Document
ICSTM	Imperial College of Science Technology and Medicine
IFR	Instantaneous Filtered Radiance
kb	kilobit
kB	kiloByte
LARC	LAngley Research Centre (NASA)
LU	Leicester University
LOS	Line Of Sight
LW	Long Wave
Mb	Megabit
MB	MegaByte
NANRG	Non Averaged, Non Rectified, Geolocated
NB	Narrow Band
NERC	Natural Environment Research Council
OSTC	Office for Scientific, Technical and Cultural Affairs

PSF	Point Spread Function
qlt	quick look time
RAL	Rutherford Appleton Laboratory
RD	Reference Document
RMIB	Royal Meteorological Institute of Belgium
RGP	RMIB Gerb Processing
ROLSS	RMIB On Line Short term Services
ScaRaB	Scanning Radiometer for radiation Budget studies
SEVIRI	Spinning Enhanced Visible and InfraRed Imager
SOL	Start Of Line
SBDART	Santa Barbara Discrete ordinate Atmospheric Radiative Transfer see http://arm.mrcsb.com/sbdart
SW	Short Wave
TAR	Tape ARchive
TBC	To Be Confirmed
TBD	To Be Determined
TOA	Top Of Atmosphere
TRMM	Tropical Rainfall Measurement Mission
UKMO	United Kingdom Meteorological Office
VIRS	VIsible and InfraRed Scanner
wrt	with respect to
WWW	World Wide Web

2.2 Definition of terms

Autorised Users

Authorised users will include RMIB, members of the GIST, GERB operations staff based at RAL, EUMETSAT and others. In order to become an Autorised user, users will be required to register with RMIB according to the rules established by the GERB Project Steering Group (TBC). Once the registration is approved the user will be able to obtain products from the ROLSS, and will be given their unique ROLSS account details, from which they will be able to get access to the products.

near real time (or NRT or nrt)

Between EUMETSAT and the GGSPS near real time means that the GGSPS at RAL will receive GERB data within 60 minutes (TBC) of the actual time at which the data was generated on board the GERB instrument.

quick look time (or QLT or qlt)

Between the GGSPS and RMIB, quick look time means that the RMIB will receive GERB data products within 4 hours of the actual time at which the corresponding data was generated on board the GERB instrument.

short term

Short term data usage refers to usage of the data within one month after their measurement.

long term

Long term data usage refers to usage of the data more than one month after their measurement.

Reference Earth Ellipsoid

(TBD)

GERB data loss

A GERB data loss is one for which the L1.5 radiances have not been obtained within the QLT.

SEVIRI data loss

A SEVIRI data loss is one for which the L1.5 SEVIRI images have not been received through the HRIT system within the QLT.

climate data

GERB climate data means the GERB products that are generated at RMIB for long term archival and data distribution at RAL.

near real time data

Near real data means the GERB products that are generated at RMIB and distributed for short term usage through the ROLSS server.

ROLSS server

The ROLSS server will be the RMIB based ftp server for near real time data distribution.

near real time processing

Near real time processing will be the processing that has to be done at RMIB as soon as a GERB or SEVIRI data file arrives.

daily, weekly, monthly processing

Daily, weekly, monthly processings will be the processings that have to be done at RMIB less frequently than the near real time processing, but that still need to be done on a regular basis.

casual processing

Casual processings will be those that have to be done at RMIB infrequently and irregularly, e.g. calibration table updates.

solar

Solar means relating to reflected solar radiation only.

thermal

Thermal means relating to emitted thermal radiation only

short wave

Short wave means radiation from the wavelengths below a cutoff wavelength of approximatively 4 micron.

long wave

Long wave means radiation from the wavelengths above a cutoff wavelength of approximatively 4 micron.

total wave

Total wave radiation means combined short wave and long wave radiation.

unfiltered

Unfiltered refers to a spectral integral of either solar or thermal radiation without spectral attenuation.

'GERB filtered' or simply 'filtered'

GERB filtered refers to a spectral integral, either over the short wave or over the long wave or over the total wave spectral interval, of radiation multiplied (filtered) with the GERB spectral response.

imager resolution

Imager resolution refers to SEVIRI pixel resolution

high resolution

HIgh resolution refers to 3 x 3 SEVIRI pixel resolution, this the highest resolution at which fluxes are derived

GERB resolution

GERB resolution refers to GERB footprint resolution

SEVIRI based products

SEVIRI based products refers to broadband radiance or flux estimates estimated from SEVIRI narrowband pixel data only.

level 2 fluxes

Level 2 fluxes refers to fluxes derived from combined GERB and SEVIRI data.

spectral unfilter factor

Ratio between the unfiltered broadband radiance and the filtered broad band radiance.

angular conversion factor

Ratio between the broad band flux and the unfiltered broad band radiance.

correction factor of SEVIRI by GERB

Ratio of the filtered broad band radiance measured by GERB and the same quantity model based on SEVIRI narrow band radiances.

3 Angular Dependency Model for Thermal Radiation

3.1 Introduction

Angular dependency models for the thermal radiation are needed to convert the broadband unfiltered thermal radiance L_{th} into broadband unfiltered thermal flux F_{th} (or OLR). This conversion is realized using the well-known equation:

$$F_{th} = \frac{\pi L_{th}}{R} \tag{1}$$

where R is the anisotropic factor which is mainly dependent on the viewing zenith angle θ (the limb darkening function). The anisotropic function $R(\theta)$ is obviously dependent on the type of atmosphere and surface condition.

Differents sets of LW angular dependency models can be found in the literature for various kinds of scenes. The ERBE empirical longwave models are described in(Suttles et al., 1989). Improved set of models are derived from the CERES–TRMM instrument(Loeb et al., 2003).

However, the GERB angular conversion does not use these emprical models but theoretical models developed at RMIB. These models are not selected by an explicit scene identification (for example 'clear sky ocean') but instead through the analysis of the NB radiances of the SEVIRI imager (Schmetz et al., 2002). The main reason for this is that the RMIB GERB Processing (RGP) does not include GERB footprint scene identification during nighttime. Indeed, the explicit scene identification (Clerbaux and Dewitte, 1999) implemented to select the SW model is mainly based on the SEVIRI visible channels and does not work during the night.

The development of the thermal radiation angular models at RMIB is described in the next sections.

3.2 Physic Statement

The radiation field at the TOA due to thermal emission is supposed to have symmetry of revolution according to the local vertical (axisymmetric atmosphere). So, the inference of the TOA outgoing thermal flux F_{th} from the TOA unfiltered thermal radiance L_{th} is only dependent on the viewing zenith angle and not on the position of the Sun. It represents mainly the limb darkening function of the Earth-atmosphere system ('scene'). The limb darkening function depends mainly on the atmospheric state and cloudiness. The surface emission is isotropic in good approximation[1].

3.3 Data set of TOA radiation fields

Thermal radiation fields are generated at RMIB using the SBDART (Ricchiazzi et al., 1998) plane-parallel radiative transfer model. For a set of 4632 different Earth/atmosphere conditions, the radiation field $L(\theta_v)$ is simulated at the viewing zenith angles:

[1]Except for example for a water surface at grazing angles.

$$\theta = \{0°, 5°, 10°, 15°, 20°, ..., 80°, 85°\} \quad (2)$$

The corresponding thermal flux F is also evaluated by the radiative transfer model. The Earth/atmosphere system is featured by surface parameters (skin temperature and emissivity), atmospheric profiles (T, p, C_{H_2O} and C_{O_3}), trace gaze concentration and cloud conditions. Up to 3 different cloud layers variation in height, phase and concentration. The generation of this data set is fully described in the RMIB technical note MSG-RMIB-GE-TN-0030 (Clerbaux, 1999).

The following problems have been detected with our simulations:

- For each spectral simulation, the surface emissivity ϵ is a random number with uniform distribution of probability in the range $[0.85 : 1]$. The spectral dependency of the emissivity $\epsilon(\lambda)$ is not simulated.
- High and semi-transparent clouds (cirrus) are represented in the data set but in an unsufficient proportion (only 5% of the simulations).

The figure hereafter illustrate the simulations in the scatterplot (L, R) at nadit, 50° viewing zenith angle and at 75° .

Illustration

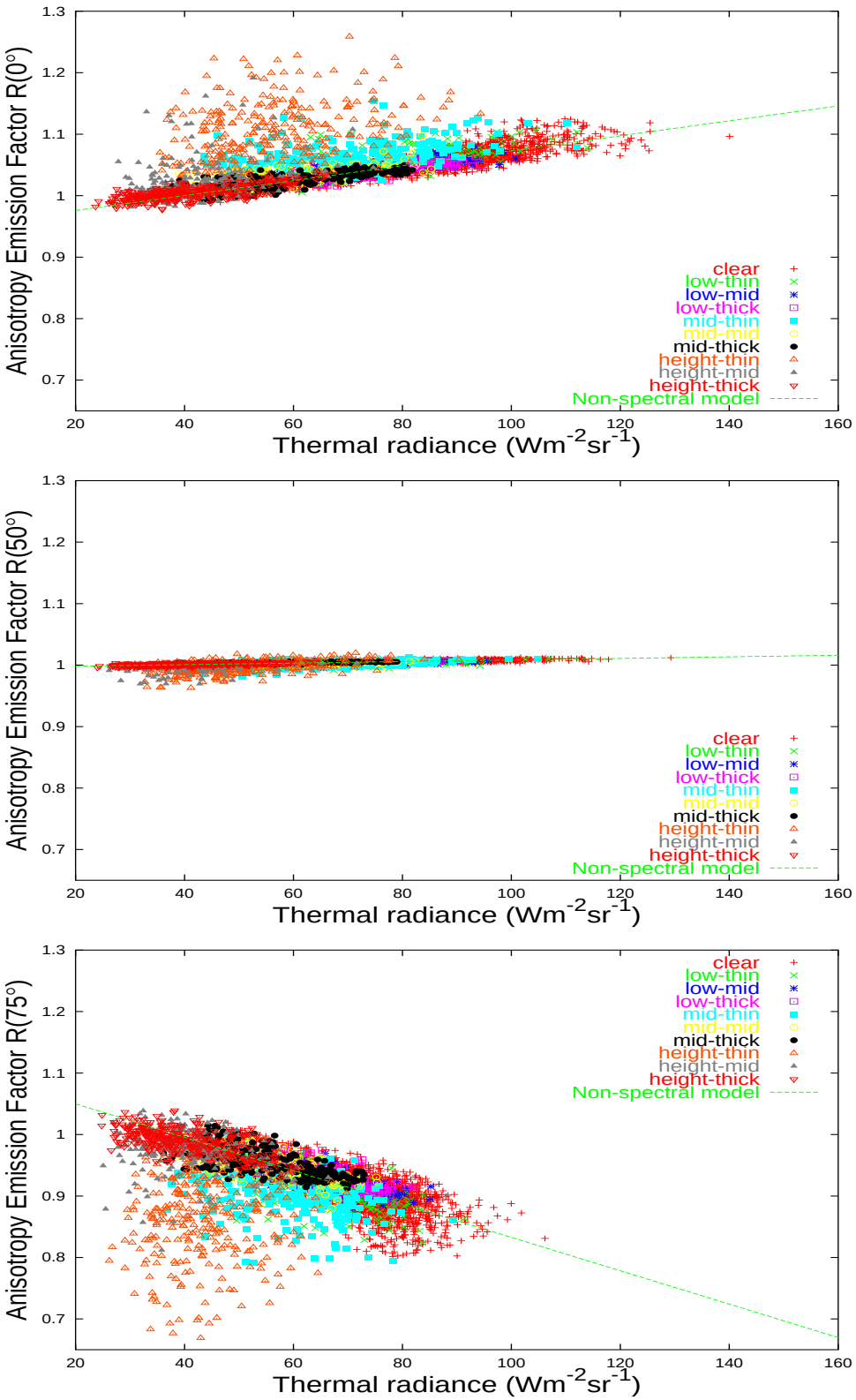

3.4 Scene Independent ADM

This is the simplest possible model with an anisotropic factor solely dependents on the viewing zenith angle θ. Using our data set to parameterize the model and evaluate the residual error gives (the last column is the residual error when the cirrus clouds are not taken into account):

theta	R(theta)	RMS err	RMS err (no cirrus)
0.0	1.042252	2.988176	2.159197
5.0	1.041920	2.961136	2.143188
10.0	1.040913	2.880082	2.095073
15.0	1.039204	2.744810	2.014217
20.0	1.036771	2.554099	1.898827
25.0	1.033591	2.305820	1.745822
30.0	1.029621	1.998010	1.551274
35.0	1.024785	1.630196	1.310517
40.0	1.018980	1.206227	1.017541
45.0	1.012091	0.752331	0.664913
50.0	1.003959	0.479000	0.259918
55.0	0.994325	0.875014	0.352507
60.0	0.982795	1.615379	0.982564
65.0	0.968803	2.528147	1.791331
70.0	0.951493	3.629568	2.834213
75.0	0.929247	5.008252	4.232606
80.0	0.898600	6.883796	6.242241
85.0	0.851513	10.077420	9.681129

At this stage we see that, **for thermal radiation, the error introduced by the flux inference from radiance is strongly depend on the viewing zenith angle**. This error seems to be minimal near 50 degrees. This fact is explained as follows: for small viewing angles (nadir view) the measured radiance is mainly the one emitted by the surface (or other optically thick objects like clouds) and the influence of atmospheric absorption/emission is small. On the other hand, at grazing angles, the radiance contains an important atmospheric contribution due to the great optical path through the atmosphere and the contribution of ground emission vanishes. At mid–value viewing angles ($\theta \approx 50^o$), the measured radiance is a good averaging of these two effects and then also a good estimator to infer the flux.

The mean hemispherical radiance L_{th}^{hemi} is defined as:

$$L_{th}^{hemi} = \frac{F_{th}}{\pi}$$

the radiance L_{th} measured at nadir is statistically higher than L_{th}^{hemi} because the surfaces have higher temperature than high level atmospheric layers. So, the anisotropic factor should be $R > 1$. On the other hand, for grazing angles, the measured radiance L_{th} is usually smaller than L_{th}^{hemi} and the anisotropic factor should be $R < 1$. These results are in good accordance with (Otterman et al., 1997), in particular for the "angle of equivalence" (where the radiance is equal to L_{th}^{hemi}) which is near 52° for a broadband radiometer[2].

[2]The angle of equivalence varies slowly with wavelength for NB measurements.

3.5 $R(\theta, L_{th})$ model

As we can see on the (L, R) scatterplots, the anisotropic factor exhibits a clear linear dependency with the broadband radiance:

$$R = A(\theta) + B(\theta)\, L_{th}$$

Using our data set to parameterize the model and evaluate the residual error gives:

theta	A(theta)	B(theta)	RMS err	RMS err (no cirrus)
0.0	0.951587	0.001215	2.691914	0.994122
5.0	0.951934	0.001206	2.666312	0.987068
10.0	0.952984	0.001181	2.588677	0.965712
15.0	0.954764	0.001137	2.457314	0.929444
20.0	0.957321	0.001074	2.270813	0.877208
25.0	0.960728	0.000990	2.028118	0.807417
30.0	0.965085	0.000883	1.727422	0.717850
35.0	0.970532	0.000749	1.366131	0.605567
40.0	0.977254	0.000583	0.945065	0.466996
45.0	0.985510	0.000379	0.493644	0.299634
50.0	0.995657	0.000127	0.385370	0.130812
55.0	1.008197	-0.000187	0.950864	0.251153
60.0	1.023863	-0.000582	1.705074	0.586953
65.0	1.043764	-0.001092	2.586225	1.044396
70.0	1.069637	-0.001770	3.600071	1.671033
75.0	1.104210	-0.002715	4.786055	2.579317
80.0	1.150541	-0.004103	6.263674	4.051432
85.0	1.188372	-0.006000	8.371407	7.107339

This simple model explains most of the variability in anisotropic factor. The residual error on R is about 1% at nadir view when the cirrus clouds are not accounted for. Unfortunatelly, the model does not perform well in case of cirrus clouds.

channel name	type	μm_i	σ_i	lower (1%)	upper (99%)
IR 3.9	window	$3.92\mu m$	$0.191\mu m$	$3.48\mu m$	$4.36\mu m$
IR 6.2	WV	$6.25\mu m$	$0.301\mu m$	$5.35\mu m$	$7.15\mu m$
IR 7.3	WV	$7.35\mu m$	$0.217\mu m$	$6.85\mu m$	$7.85\mu m$
IR8.7	window	$8.70\mu m$	$0.174\mu m$	$8.30\mu m$	$9.10\mu m$
IR9.7	O_3	$9.66\mu m$	$0.122\mu m$	$9.38\mu m$	$9.94\mu m$
IR 10.8	window	$10.8\ \mu m$	$0.435\mu m$	$9.8\ \mu m$	$11.8\mu m$
IR12	window	$12.0\ \mu m$	$0.435\mu m$	$11.0\ \mu m$	$13.0\mu m$
IR 13.4	CO_2	$13.4\ \mu m$	$0.435\mu m$	$12.4\ \mu m$	$14.4\mu m$

Table 1: The SEVIRI channels in the thermal part of the spectrum : EUMETSAT names, type of channel, mean and standard deviation when spectral filters are modeled with Gaussian shape, expected lower and upper limits

3.6 ADM with Implicit Scene Identification using SEVIRI

3.6.1 Channels, calibration and accuracies

The MSG imager, SEVIRI, performs 8 spectral measurements in the thermal part of the spectrum. The table 1 gives the characteristics of these channels. This information is extracted from the SEVIRI Science Plan (1998, EUMETSAT Doc. EUM/MSG/PLN/193, 68 pp. [Available online at www.eumetsat.de.]). During the day, the IR 3.9 channel is contaminated by reflected solar radiation. For this reason, this channel is not used to estimate the anisotropic conversion factor R from narrow-band radiances. The accuracies of these narrow-band radiances are estimated at 2% (standard deviation of the noise level + calibration accuracy).

With SEVIRI, the "implicit scene identification" problem becomes to find the best-suited function for the anisotropic factor:

$$R_\theta \;=\; R_\theta(\, L_{6.2\mu}, L_{7.3\mu}, L_{8.7\mu}, L_{9.7\mu}, L_{10.8\mu}, L_{12\mu}, L_{13.4\mu}) \tag{3}$$

3.6.2 Model with 7 inputs

After various trails (Clerbaux et al., 2003) not described here, a second order regression was selected for Eq.3. A second order regression on 7 inputs contains $1 + N + N(N-1)/2 = 36$ parameters.

3.6.3 Model with 4 inputs

After careful analysis, it appears that (a part of) the hot desert problem is introduced by the fact that the SBDART simulations have been performed using spectrally constant surface emissivity, which is not the case for the unvegetated land surface.

A new regression has been derived using as inputs the limited set of channels (WV 6.2μm, IR 10.8μm, IR 12μm, IR 13.4μm) which have emissivity less subject to surface type. The methodology and simulations are exactly the same as for the general regression, only a reduced set of inputs is used in the regression.

This new model has been evaluated (see the validations hereafter) and it appears that it performs better that the initial one, even over ocean surface. We therefore propose to replace the 7-inputs model by this new 4-inputs model.

3.6.4 Cirrus model

It is possible to derive and apply specific anisotropic model for high semi-transparent clouds. Such a model is proposed in the RMIB technical note MSG-RMIB-GE-TN-0039(Clerbaux, 2006). This was not implemented in the processing as not sufficiently mature.

3.6.5 Residual angular dependency

The methodology of Steven Dewitte is used to check the residual angular dependency. Details about the method and data is given in MSG-RMIB-GE-TN-0039(Clerbaux, 2006). The difference GERB-CERES is analyzed as a function of the VZA as:

$$F_{GERB} - F_{CERES} = a(F_{GERB}) \frac{52.5 - VZA_{GERB}}{52.5} + b(F_{GERB}) \tag{4}$$

The parameters $a(F_{GERB})$ and $b(F_{GERB})$ are estimated over $20 W m^{-2}$ bins of F_{GERB}. If the angular modeling is correctly performed, the factors a should be close to 0 for all the OLR bins (b may differ due to calibration/unfiltering).

The Figure (1) gives the variation of the a factor according to F_{GERB}. The improvement of the angular modeling is well visible in July and December.

3.7 Discussion

For the first GERB data release (Edition 1), the 4 inputs model will be use, although this model is known to introduce error in the convective region, probably due to the high semi-transparent cloudiness there.

The error introduced on the fluxes is strongly dependent on the viewing zenith angle θ and vanishes nearly for angles close to $\theta s \approx 52^o$ (Europa, ...). At nadir (Africa), the thermal flux from radiance inference process is characterized by an error bellow $\epsilon_r < 3\%$, except for high semi-transparent clouds.

Note that, as for the spectral modeling, all the errors are related to the dispersion in the data set of Earth-atmosphere conditions that serve as input to generate angular/spatial radiation fields at the TOA by radiative computation (Clerbaux, 1999). This dispersion can be more or less important than the real dispersion.

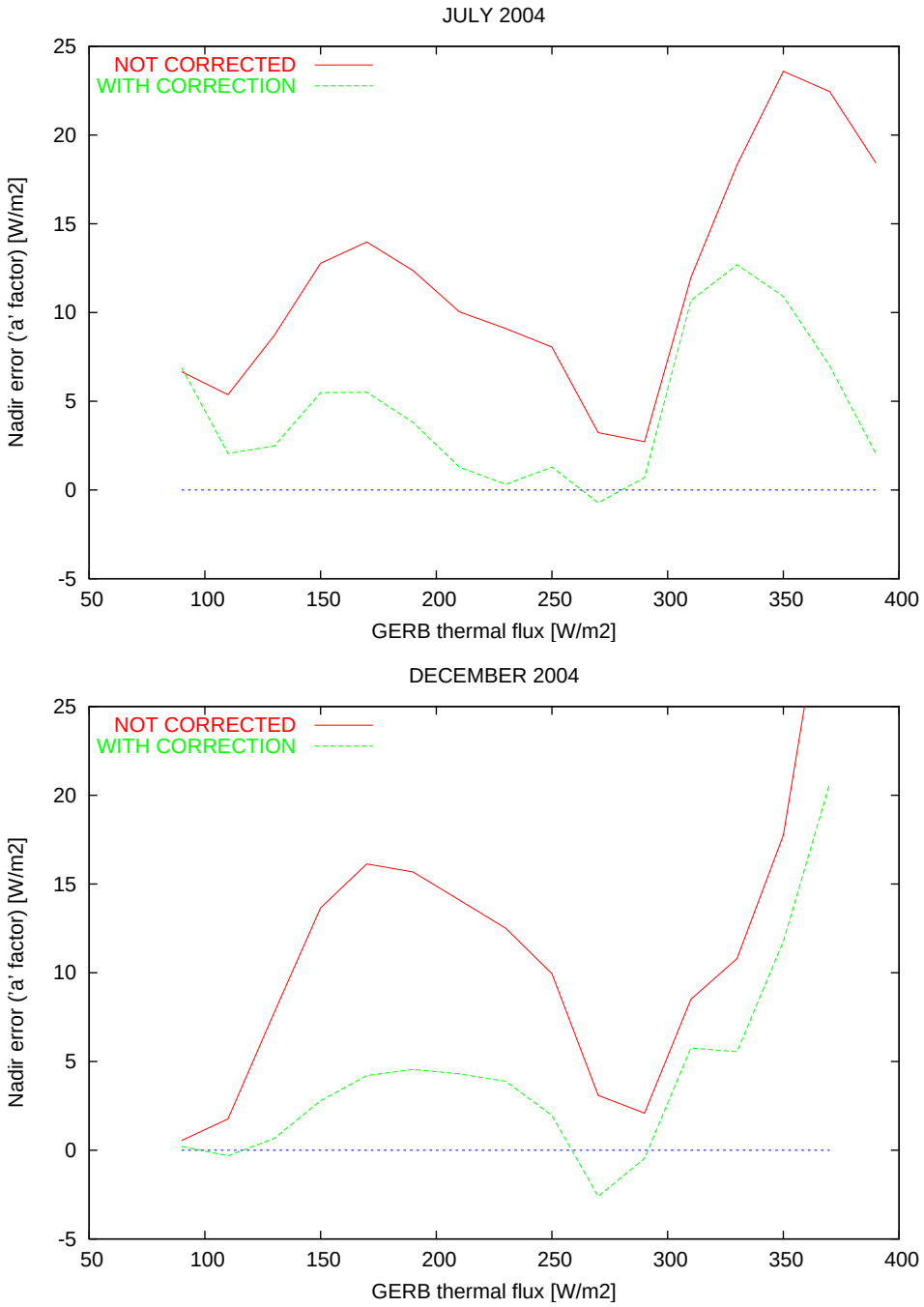

Figure 1: Residual angular dependency of the GERB OLR (factor a) according to the thermal flux.

4 The ADM for Solar Reflected Radiation Field

4.1 Introduction

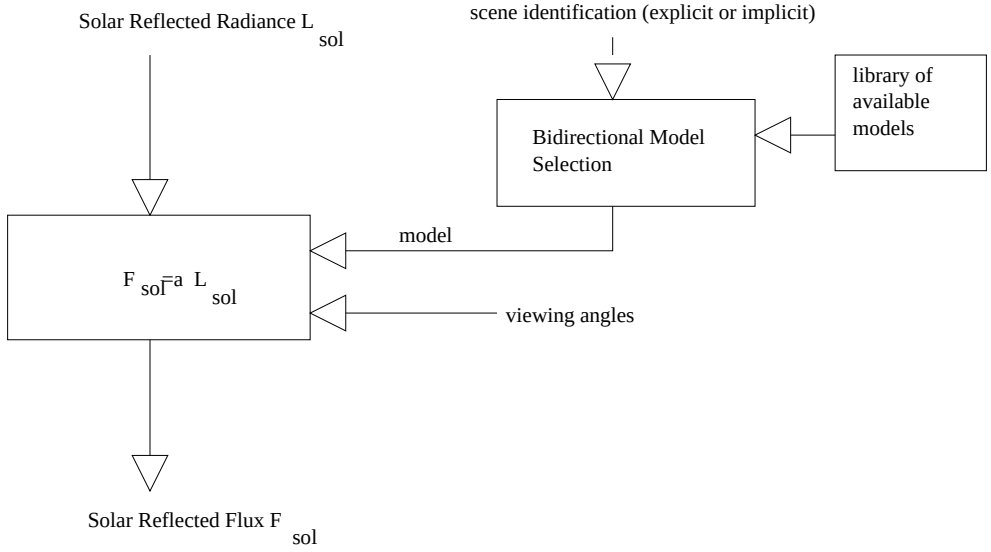

Unlike thermal processing, angular dependency models for the solar reflected radiation are not developed at RMIB in the frame of the GERB RMIB Ground Segment[3]. So, existing solar reflected ADM's are used. In this section, these models and the way to select them from the scene identification is presented.

4.2 Physic statement,

4.2.1 Solar Reflected Radiation Field

The radiance field of solar reflected radiation at the TOA is written:

$$L(\theta_s, \theta_v, \phi)\ [Wm^{-2}sr^{-1}] \tag{5}$$

where θ_s is the solar zenith angle, θ is the viewing zenith angle and ϕ is the relative azimuth angle between the sun and the satellite ($\phi = 0$ in the forward direction).

The flux at the TOA is the integral on the upper hemisphere of the radiance field:

$$F(\theta_s) = \int_{\phi=0}^{2\pi} d\phi \int_{\theta=0}^{\pi/2} d\theta\, L(\theta_s, \theta_v, \phi)\, \cos\theta\, \sin\theta \tag{6}$$

[3]The development of ADM for solar radiation is a heavy work due to the great number of physical processes that have to be taken into account in radiation transfer modeling. The angular geometry is also more complex than for thermal radiation because in the solar region the sun location influes on the angular distribution of the radiation field.

A particular condition for the Earth-atmosphere system (for example 'clear dark desert') is characterized by its TOA albedo $A(\theta_s)$:

$$A(\theta_s) = \frac{F(\theta_s)}{\cos\,\theta_s\, E_0} \tag{7}$$

and its anisotropic function R:

$$R(\theta_s, \theta_{v,}\phi) = \frac{\pi\, L(\theta_s, \theta_v, \phi)}{F(\theta_s)} \tag{8}$$

where E_0 in Eq.(7) is the solar constant corrected for the Earth-sun distance.

4.2.2 Flux inference from radiance

To retrieve the solar reflected flux F_{sol} from the solar reflected radiance L_{sol}, one has to evaluate the value of the bidirectional function R and then use the relation (derived from 8):

$$F_{sol} = \frac{\pi}{R(\theta_s, \theta, \phi)}\, L_{sol} \tag{9}$$

4.2.3 Models

Each Earth-atmosphere scene is featured by its own bidirectional reflection R and albedo A functions. Angular radiation modeling consists to merge into classes scenes that have the same bidirectional and albedo behavior and to derive averaged bidirectional reflection R_c and albedo A_c functions for these classes. After modeling, the $R_c(\theta_s, \theta, \phi)$ and $A_c(\theta_s)$ functions can be expressed as analytical functions (Manalo-Smith et al., 1998) or as table of values for sets of angle bins (Loeb et al., 2003; Suttles et al., 1988).

4.2.4 Explicit versus Implicit Scene Identification

Explicit scene identification As the angular dependency models (R and A) are derived for a set of classes (e.g. 12 classes for the ERB ADM), a scene identification is necessary in the GERB ground segment. The scene identification based on the imager (METEOSAT-7 or SEVIRI) is described in the technical note MSG-RMIB-GE-TN-0007(Clerbaux and Dewitte, 1999). This scene identification process allows to select, among the various available ADMs, of the model with angular behavior the closest to the one of the scene. Interpolation may also be done between available angular models.

Implicit Scene Identification The choice of the best model to convert the solar reflected radiance L_{sol} into the flux F_{sol} can also be done by selecting, among the various ADMs available, the one that predicts the radiance L_c the closest to the measured radiance L_{sol}. From equations 8 and 7 the predicted radiance for the class c is:

$$L_c = \frac{\pi}{R_c(\theta_s, \theta, \phi)} A_c(\theta_s) \cos\theta_s E_0 \quad (10)$$

This approach is simple because an explicit scene identification is not needed but leads to poor results when: the number of available models is important ($N \gg 10$) or when the viewing geometry (θ_s, θ, ϕ) is not discriminant (for example, at grazing angles the Rayleigh scattering due to atmospheric constituent trends to equalize the radiances modeled for the various classes). This approach is not planned to be used in the RMIB GERB Ground Segment.

4.3 RGP Scene Identification

The RGP scene identification is fully described in RMIB technical note MSG-RMIB-GE-TN-0007(Clerbaux and Dewitte, 1999). It includes 2 kinds of products :

- the surface type which does not change with time. For each footprint, the percentage of the 6 type of surface is given. The snow percentage will be added latter (TBD) (with temporal variations).
- the cloud products derived from the cloud analysis process: cloud fraction [%], cloud optical depth (log averaging over the cloudy part of the pixel) and averaged cloud phase. An additonal flag is activated in case of pixel shadowing by neighnour cloud.

4.4 The ADM derived from the ERB Experiment

4.4.1 Available Models

Short wave angular models have been developed based on data collected by the ERB scanner on-board Nimbus-7 and from GOES. These models are well-known by the climatology community working on the Earth Radiation Budget problems and are fully described in (Suttles et al., 1988). Models were derived for 12 classes :

scene id	description
1	clear ocean
2	clear land
3	clear snow
4	clear desert
5	clear land-ocean mix
6	partly cloudy over ocean
7	partly cloudy over land or desert
8	partly cloudy over land-ocean mix
9	mostly cloudy over ocean
10	mostly cloudy over land or desert
11	mostly cloudy over land-ocean mix
12	overcast

The cloudiness for these models is related to the percentage of cloudy pixels within the broadband radiometer footprint as follow:

cloud type	percentage of cloudy pixels
clear	<5%
partly	5% to 50%
mostly	50% to 95%
overcast	>95%

4.4.2 Model Selection from Scene Identification Product

The dark and bright vegetation classes are asociated with the ERBE land class. The dark and bright desert classes are associated with the ERBE desert class. The fottprint having water fraction between 5% and 95% are associated with the ERBE mix land-ocean class.

The ERB cloud cover type is selected according to the cloud fraction within a SHI pixel (3*3 SEVIRI pixels) using:

cloud type	number of cloudy pixels
clear	0
partly	1, 2 3 or 4
mostly	5,6,7 or 8
overcast	9

4.5 The ADM derived from the CERES-TRMM experiment

4.5.1 Available Models

These models have been developped by Norman Loeb and the CERES inversion team at NASA Langley Research Center. The models are based of 8 months of the observations done by the Clouds and Earth's Radiant Energy System (CERES, Wielicki et al., 1996) instrument on the TRMM satellite.

Models are derived for 6 surface types: ocean, dark and bright vegetation, dark and bright desert, snow. The cloudiness is discrimated according to: the cloud phase (water cloud or ice particles clouds), the cloud fraction over the footprint and the average cloud optical depth over the cloudy part of the footprint.

4.5.2 Model Selection from Scene Identification Product

The surface type is extract from a map of CERES ST built using 1km data as described in MSG-RMIB-GE-TN-0024(Clerbaux, 2003). In case of mix pixels, the anisotropic factor is obtain with the adequate weighting (Bertrand et al., 2005; Suttles et al., 1988):

$$R(\theta_0, \theta, \phi) = \frac{\Sigma_i w_i A_i(\theta_0) R(\theta_0, \theta, \phi)}{\Sigma_i w_i A_i(\theta_0)} \tag{11}$$

where w_i is the fraction of surface type i in the footprint and A_i and R_i the corresponding TOA albedo and bidirectional distribution function.

The model selection according to the RGP cloud analysis products is quite simple.

4.5.3 Interpolation

A simple trilinear interpolation is realized on the R values. This is not exactly what is adviced by the CERES team who advocates to interpolate separately the modem albedo and BRDF. We do implement the ADM normalisation.

At this time there is no interpolation between in cloud fraction, cloud phase and cloud optical depth.

4.6 Additional Models

Additional models are added to the ERB or CERES models in the frame of the GERB RMIB ground segment. These models are described hereafter.

4.6.1 Lambertian model

The lambertian model is defined by:

$$R(\theta_s, \theta_v, \phi) \; = \; 1 \tag{12}$$

$$A(\theta_s) \;=\; undefined \tag{13}$$

The lambertian model is used in the shadowed regions. Shadowed pixels may appear for grazing solar zenith angle (dawn and dusk) at the borders of cloud formation (specially near high level clouds). The shadow flag is a separated product generated by the cloud analysis which is a subsystem of the scene identification described in (Clerbaux and Dewitte, 1999). This model is also used to convert radiance in flux for solar zenith angle higher than 90°.

4.6.2 Mean Earth-atmosphere model

The mean Earth-atmosphere model is defined as:

$$R(\theta_s, \theta_{v,}\phi) \;=\; \sum_{c=1}^{N} w_c \, R_c(\theta_s, \theta_{v,}\phi) \tag{14}$$

$$A(\theta_s) \;=\; undefined \tag{15}$$

The anisotropy function R for this model is a simple weighting of the available models for the same angular configuration (θ_s, θ, ϕ). $\{w_c\}$ are the a-priori probabilities of occurence of the classes:

$$\sum_{c=1}^{N} w_c \;=\; 1$$

This model will be used for pixels where scene identification products are not available or not complete.

4.6.3 Sun Glint Model

Sun glint may occur on clear sky ocean surfaces when the tilt angle[4] is under $\theta_t < 25^o$. In the sun glint region, the radiance L_{sol} increases strongly due to specular reflection on the ocean surface. The retrieval of the TOA solar reflected flux F_{sol} from this radiance L_{sol} leads to important errors. Indeed, Eq.(9) shows that the flux is computed as the division of two great terms : L_{sol} and $R_{ocean}(\theta_s, \theta, \phi)$.

In the sun glint area it is more accurate to estimate the TOA flux using the modeled ocean albedo instead of the measured radiance:

$$F_{sol} \;\neq\; \frac{\pi}{R_{ocean}(\theta_s, \theta, \phi)} \, L_{sol} \tag{16}$$

$$F_{sol} \;= A_{ocean}(\theta_s) \, \cos\,\theta_s \, E_0 \tag{17}$$

[4]The tilt angle θ_t is the angle between the direction of sun specular reflection (forward direction) and the direction of the satellite.

4.6.4 Data Masking in the GERB products

Althrough the angular conversion is performed whatever are the geometry, the SW flux is set to the error value for $\theta_0 > 80^\circ$ (grazing illumination), $\theta > 80^\circ$ (grazing observation) or $\theta_t < 15^\circ$ (sun glint condition).

4.7 Discussion

For the first GERB data release (Edition 1), the CERES-TRMM models are used as described. Analysis of pre-released data did not indicated any particular radiance–to–flux conversion problem for the solar reflected radiation.

References

C. Bertrand, N. Clerbaux, A. Ipe, S. Dewitte, and L. Gonzalez. Angular distribution models anisotropic correction factors and mixed clear scene types: a sensitivity study. *IEEE Transactions on Geoscience and Remote Sensing*, 43(1):92–102,, 2005.

N. Clerbaux. Generation of a data base of TOA spectral radiance fields. Technical Note MSG-RMIB-GE-TN-0030, RMIB, December 1999.

N. Clerbaux. RGP-SP : Data dictionary. Technical Note MSG-RMIB-GE-TN-0024, RMIB, 2003.

N. Clerbaux. Proposal to modify the gerb longwave adm. Technical Note MSG-RMIB-GE-TN-0039, RMIB, January 2006.

N. Clerbaux and S. Dewitte. RMIB GERB processing - SEVIRI processing : Scene identification. Reference Document MSG-RMIB-GE-TN-0007, RMIB, 1999.

N. Clerbaux, S. Dewitte, L. Gonzalez, C. Bertand, B. Nicula, and A. Ipe. Outgoing longwave flux estimation: Improvement of angular modelling using spectral information. *Remote Sensing of Environment*, 85:389–395, 2003.

J. Harries and GIST. The geostationary earth radiation budget project. *Bulletin of the American Meteorological Society*, 86(7):945–960, 2005.

N.G. Loeb, N.M. Smith, S. Kato, W.F. Miller, S.K. Gupta, P. Minnis, and B.A. Wielicki. Angular distribution models for top-of-atmosphere radiative flux estimation from the clouds and the earth's radiant energy system instrument on the tropical rainfall measuring mission satellite. part i: Methodology. *Journal of Applied Meteorology*, 42:240–265, 2003.

N. Manalo-Smith, G. L. Smith, S. N. Tiwari, and W. F. Staylor. Analytic forms of bidirectional reflectance functions for application to earth radiation budget studies. *Journal of Geophysical Research*, 103(.12):19733–19752, 1998.

J. Otterman, D. Starr, T. Brakke, R. Davies, H. Jacobowitz, A. Mehta, F. Chéruy, and C. Prabhakara. Modeling zenith-angle dependence of outgoing longwave radiation: Implication for flux measurements. *Remote Sensing of Environment*, 62:90–100, 1997.

P. Ricchiazzi, S. Yang, C. Gautier, and D. Sowle. SBDART: A research and teaching software tool for plane-parallel radiative transfer in the earth's atmosphere. *Bulletin of the American Meteorological Society*, 79(10):2101–2114, 1998. available at http://arm.mrcsb.com/sbdart.

J. Schmetz, P. Pili, S. Tjemkes, D. Just, J. Kerkmann, S. Rota, and A. Ratier. An introduction to meteosat second generation (msg). *Bulletin of the American Meteorological Society*, 83: 977–992, 2002.

J. T. Suttles, R. N. Green, G. L. Smith, B. A. Wielicki, I. J. Walker, V. R. Taylor, and L. L. Stowe. Angular radiation models for earth-atmosphere system. Volume II– longwave radiation. Reference Publication 1184, NASA, 1989.

J.T. Suttles, R.N. Green, P. Minnis, G.L. Smith, W.F. Staylor, B.A. Wielicki, I.J. Walker, D.F. Young, V.R. Taylor, and L.L. Stowe. Angular radiation models for earth-atmosphere system: Volume i - shortwave radiation. Reference Publication 1184, NASA, July 1988.

B. A. Wielicki, B. R. Barkstrom, E. F. Harrison, R. B. Lee III, G. L. Smith, and J. E. Cooper. Clouds and the earth's radiant energy system (CERES): An earth observing system experiment. *Bulletin of the American Meteorological Society*, 77:853–868, 1996.